Axisymmetric Electromagnetic Resonant Cavity Solution by a Meshless Local Petrov-Galerkin Method

Ramon D. Soares[1], Renato C. Mesquita[2], and Fernando J. S. Moreira[1]

[1] Department of Electronics Engineering
Federal University of Minas Gerais (UFMG), Belo Horizonte, MG 31270-901, Brazil
ramon_dornelas@yahoo.com.br, fernandomoreira@ufmg.br

[2] Department of Electrical Engineering
Federal University of Minas Gerais (UFMG), Belo Horizonte, MG 31270-901, Brazil
renato@ufmg.br

Abstract ― This work describes a meshless approach to obtain resonant frequencies and field distributions in axisymmetric electromagnetic cavities. The meshless local Petrov-Galerkin is used with shape functions generated by moving least squares. Boundary conditions are imposed by a collocation method that does not require integrations. The proposed analysis has simple implementation and reduced computational effort. Results for TE and TM modes of cylindrical and spherical cavities are presented and compared with analytical solutions.

Index Terms ― BOR (bodies of revolution), electromagnetic cavities, LBIE (local boundary integral equation), and MLPG (meshless local Petrov-Galerkin).

I. INTRODUCTION

Meshless methods are a class of numerical methods able to solve problems governed by partial differential equations (PDE), as other methods vastly used by the computational electromagnetic (CEM) community like the finite element method (FEM) and the finite difference method (FDM). The FDM is usually employed to solve problems in time domain, generating the well-known finite difference time domain (FDTD) [1]. FEM, on the other hand, is generally used to solve electromagnetic problems in frequency domain. Both methods need a mesh (FEM) or a grid (FDTD) to attain a numerical solution.

A mesh generation with strict quality restrictions required by numerical methods is a very demanding task, especially for very complicated geometries and for three-dimensional (3D) problems. For this reason, alternative numerical techniques without meshes or grids are sought. In meshless methods, the numerical solution is obtained without setting up any kind of grid or mesh. From a computational perspective, FEM requires more time in its mesh setup, while meshless methods demand on its matrix computation due to the complexity of their shape function construction.

Meshless methods can be classified in two categories: methods based on strong forms and those based on weak formulations. In strong-form methods, the governing partial differential equations (PDEs) are directly discretized using simple collocation techniques. These methods are computationally efficient and have simple implementation; but they are often unstable, not robust, and inaccurate [2]. Meshless methods based on collocation are generally implemented using smoothed particle hydrodynamics for electromagnetics (SPEM) formulations [3] or radial basis functions [4, 5, and 6].

In order to use methods based on weak formulations, it is necessary to construct a weak equation, which is obtained by applying the residual method to the PDE [2]. Galerkin or Petrov-Galerkin methods can be used to discretize the weak equation, resulting in methods more

Submitted On: May 31, 2011
Accepted On: October 16, 2011

robust, stable, and with higher convergence rates than collocation techniques [2].

The element free Galerkin method (EFGM) is a global weak formulation, which has been successfully applied in the solution of wave scattering problems [7]. The main drawback of the EFGM is that it requires a background mesh to perform numerical integrations. Recently, meshless local Petrov-Galerkin (MLPG), which is a local weak-form method and does not use a mesh even for integration, has been used to solve wave propagation [8] and 3D static problems [9].

The present work extends the MLPG procedures presented in [8 and 9] to determine the resonant frequencies and field distributions inside axisymmetric cavities. Similar problems have been solved in [4 and 5] using meshless collocation methods. Our work adopts MLPG, which is a weak-form method that, in principle, has better precision and numerical stability when compared with collocation methods [2].

II. PROBLEM FORMULATION

The vectorial Helmholtz equation for a source-free region containing a material characterized by its relative permittivity ϵ_r and permeability μ_r is given by [10]

$$\nabla \times \left(\frac{1}{\epsilon_r} \nabla \times \vec{H}\right) - {k_0}^2 \mu_r \vec{H} = 0, \qquad (1)$$

where $k_0^2 = \omega^2 \epsilon_0 \mu_0$ and k_0 is the free-space wavenumber.

We first make the assumption that the field distribution is also axisymmetric, i.e., the magnetic field in (1) has only the ϕ-component and varies only in ρ and z directions ($\vec{H} = H_\phi(\rho, z)\hat{\phi}$). This assumption is applied in (1) and results in a TM scalar formulation:

$$\frac{\partial}{\partial \rho}\left[\frac{1}{\rho\epsilon_r}\frac{\partial(\rho H_\phi)}{\partial \rho}\right] + \frac{\partial}{\partial z}\left[\frac{1}{\rho\epsilon_r}\frac{\partial(\rho H_\phi)}{\partial z}\right] + k_0^2 \mu_r H_\phi = 0. \qquad (2)$$

The weak form is then obtained by the weighted residual method, multiplying (2) by a test function $\psi(\rho, z)$ and integrating the result over the domain Ω:

$$\iint_\Omega \frac{\partial}{\partial \rho}\left[\frac{1}{\rho\epsilon_r}\frac{\partial(\rho H_\phi)}{\partial \rho}\right]\psi + \frac{\partial}{\partial z}\left[\frac{1}{\rho\epsilon_r}\frac{\partial(\rho H_\phi)}{\partial z}\right]\psi dA + k_0^2 \iint_\Omega \mu_r H_\phi \psi dA = 0. \qquad (3)$$

After some mathematical manipulations [10], the weak form for the TM solution is obtained:

$$\oint_{\partial\Omega} \frac{\psi}{\rho\epsilon_r}\frac{\partial(\rho H_\phi)}{\partial n} dl - \iint_\Omega \frac{\nabla\psi \cdot \nabla(\rho H_\phi)}{\epsilon_r \rho} dA + k_0^2 \iint_\Omega \frac{\mu_r \psi(\rho H_\phi)}{\rho} dA = 0. \qquad (4)$$

The TE weak formulation is obtained from duality. A single equation mathematically expressing both TE and TM cases is written as

$$\oint_{\partial\Omega} \frac{\psi}{\rho f}\frac{\partial u}{\partial n} dl - \iint_\Omega \frac{\nabla\psi \cdot \nabla u}{f\rho} dA + k_0^2 \iint_\Omega \frac{g\psi u}{\rho} dA = 0, \qquad (5)$$

where, for TM modes, $u = \rho H_\phi$, f is the relative electric permittivity ϵ_r, and g is the relative magnetic permeability μ_r inside the cavity. For TE modes, $u = \rho E_\phi$, $f = \mu_r$, and $g = \epsilon_r$.

III. THE MESHLESS APPROACH

Equation (5) is numerically evaluated by a meshless approach, which begins by spreading nodes (field nodes) over the problem domain Ω and its boundary $\partial\Omega$ (see Fig. 1). Every node x_I has an associated shape function ϕ_I, which is different from zero only in a small region around the node I. This region is known as node I's influence domains Ω_{F_I}, as illustrated in Fig. 1. The influence domain can be of any shape (generally circular, square, or rectangular forms are adopted), as long as their union covers all the problem domain Ω. In this work, circular influence domains are employed. The local approximation of u at a point x is then given by:

$$u^h(x) = \sum_I^N \phi_I(x) u_I, \qquad (6)$$

where $I = 1, \ldots, N$ represents the nodes whose influence domains include point x and u_I are the nodal values. The set of N nodes is known as the support domain Ω_x (Fig. 1). To build the shape function we have adopted the moving least squares (MLS) method, which begins by

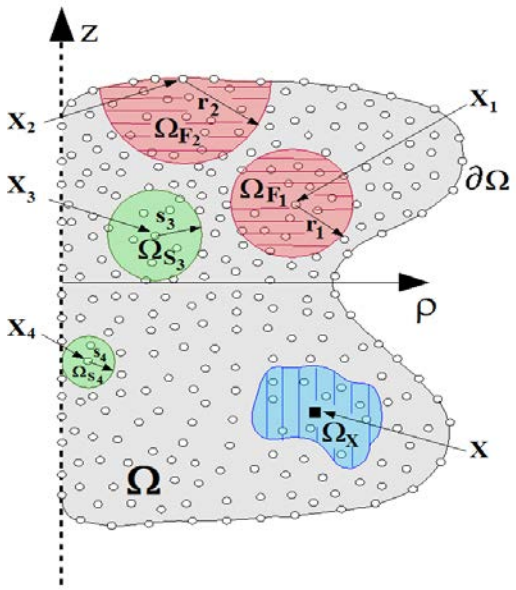

Fig. 1. A computational domain Ω and its boundaries $\partial\Omega$. The horizontal striped regions are influence domains Ω_{F_1} and Ω_{F_2} of the nodes x_1 and x_2, respectively. The non-striped regions are test domains Ω_{S_3} and Ω_{S_4} of the nodes x_3 and x_4, respectively. The vertical striped region is the support domain Ω_x of a point x.

expressing u^h as [2]

$$u^h(\mathrm{x}) = \mathbf{p}^{\mathrm{T}}(\mathrm{x})\mathbf{a}(\mathrm{x}), \qquad \forall\, \mathrm{x} \in \Omega_{\mathbf{x}}, \quad (7)$$

where $\mathbf{p}^{\mathrm{T}}(\mathrm{x}) = [p^1(\mathrm{x}), p^2(\mathrm{x}), \ldots, p^m(\mathrm{x})]$ is a complete monomial basis with m terms and $\mathbf{a}(\mathrm{x})$ is a vector containing the coefficients $a^j(\mathrm{x})$, $j = 1, 2, \ldots, m$, which are functions of the space co-ordinates $\mathrm{x} = [\rho,\ z]^{\mathrm{T}}$. For example, using a first order polynomial, $\mathbf{p}^{\mathrm{T}}(\mathrm{x})$ is given by:

$$\mathbf{p}^{\mathrm{T}}(\mathrm{x}) = [1, \rho, z], \quad \text{for } m = 3. \qquad (8)$$

The coefficient vector $\mathbf{a}(\mathrm{x})$ is determined by minimizing a weight discrete L_2-norm defined as:

$$J = \sum_{\mathrm{I}=1}^{N} w(\mathrm{d_I})\,[\mathbf{p}^{\mathrm{T}}(\mathrm{x_I})\mathbf{a}(\mathrm{x}) - \mathrm{u_I}]^2, \qquad (9)$$

where N is the number of nodes in the support domain of x and $\mathrm{x_I}$ are the coordinates of node I. The chosen weighting function is a third order spline function expressed by [2]:

$$w(d_I) = \begin{cases} \frac{2}{3} - 4{d_\mathrm{I}}^2 + 4{d_\mathrm{I}}^3 & \text{if } d_I \le \frac{1}{2} \\ \frac{4}{3} - 4d_\mathrm{I} + 4{d_\mathrm{I}}^2 - \frac{4}{3}{d_\mathrm{I}}^3 & \text{if } \frac{1}{2} < d_\mathrm{I} \le 1 \\ 0 & \text{otherwise,} \end{cases} \qquad (10)$$

where $d_\mathrm{I} = |\mathrm{x} - \mathrm{x_I}|/r_\mathrm{I}$ and r_I is the radius of the influence domain associated to node I, as shown in Fig. 1. The r_I values are obtained in a two step preprocess: (i) a small set of N_{ini} neighbor nodes for each node I is selected; (ii) the distance between node I and its furthest neighbor node ($dist_\mathrm{I}$) is evaluated and multiplied by the dimensionless size parameter α_I, defining $r_I = dist_I \cdot \alpha_I$.

The minimization of J results in [2]

$$\mathbf{a}(\mathrm{x}) = \mathbf{A}^{-1}(\mathrm{x})\mathbf{B}(\mathrm{x})\mathbf{U}, \qquad (11)$$

where $\mathbf{A}$ is the moment matrix, given by

$$\mathbf{A}(\mathrm{x}) = \sum_{\mathrm{I}=0}^{N} w(\mathrm{x} - \mathrm{x_I})\mathbf{p}(\mathrm{x_I})\mathbf{p}^{\mathrm{T}}(\mathrm{x_I}), \qquad (12)$$

the matrix $\mathbf{B}$ has the form $\mathbf{B}(\mathrm{x}) = [\boldsymbol{B_1}, \boldsymbol{B_2}, \ldots, \boldsymbol{B_N}]$, with column elements $\boldsymbol{B}_\mathrm{I}$ defined by

$$\boldsymbol{B}_\mathrm{I} = \mathrm{w}(\mathrm{d_I})\mathbf{p}(\mathrm{x_I}), \qquad (13)$$

and $\mathbf{U}$ is the vector that contains all fictitious nodal values of support domain Ω_x, $\mathbf{U} = \{\mathrm{u}_1, \ldots, \mathrm{u}_N\}^{\mathrm{T}}$.

Equation (7) can be rewritten using (11) as follows [2]:

$$u^h(\mathrm{x}) = \mathbf{p}^{\mathrm{T}}(\mathrm{x})\mathbf{A}^{-1}(\mathrm{x})\mathbf{B}(\mathrm{x})\mathbf{U} = \boldsymbol{\Phi}^{\mathrm{T}}(\mathrm{x})\mathbf{U}, \quad (14)$$

where $\boldsymbol{\Phi}(\mathrm{x})$ is the matrix of MLS shape functions corresponding to N nodes of Ω_x, written as:

$$\boldsymbol{\Phi}^{\mathrm{T}}(\mathrm{x}) = [\phi_1(\mathrm{x}), \phi_2(\mathrm{x}), \ldots, \phi_N(\mathrm{x})], \qquad (15)$$

where $\phi_\mathrm{I}(\mathrm{x})$ is the shape function of the Ith node of Ω_x. Equation (14) indicates that shape functions and, consequently, the MLS approximation depend on $\mathbf{A}^{-1}$. A well-conditioned $\mathbf{A}$ matrix is guaranteed using $\mathrm{N} \gg \mathrm{m}$ and avoiding certain singular node distributions (e.g., a collinear node distribution) [2]. Equation (14) is the matrix form of (6).

The partial derivatives of $\boldsymbol{\Phi}$ with respect to ρ are obtained as:

$$\boldsymbol{\Phi}^{\mathrm{T}}_{,\rho} = \mathbf{p}_{,\rho}{}^{\mathrm{T}}\mathbf{A}^{-1}\mathbf{B} + \mathbf{p}^{\mathrm{T}}\mathbf{A}^{-1}_{,\rho}\mathbf{B} + \mathbf{p}^{\mathrm{T}}\mathbf{A}^{-1}\mathbf{B}_{,\rho}, \quad (16)$$

where the subscript $,\rho$ denotes the parcial derivative with respect to ρ. Derivatives of the

shape function with respect to z are obtained in a similar way [2].

Figure 2 illustrates a MLS shape function for a node located at $\mathrm{x}^{\mathrm{T}} = [0,0]$, obtained using 25 nodes uniformly spread over Ω. Each node in the domain will have a similar function associated to it and the final approximation will be given by (6). The precision of the approximation depends on the node distribution, but if we define a FEM mesh and generate a MLS approximation using the FEM mesh nodes, the MLS approximation is typically more precise than FEM [2]. Figure 3 shows the first derivative of the MLS shape function with respect to ρ.

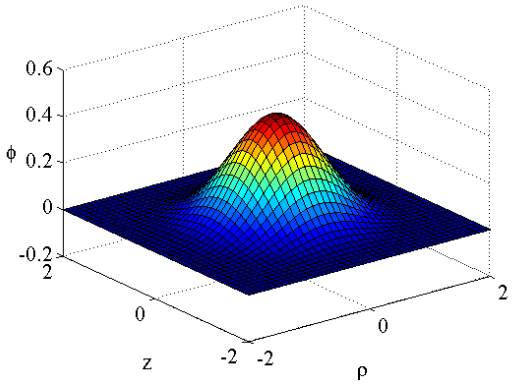

Fig. 2. Shape function, ϕ.

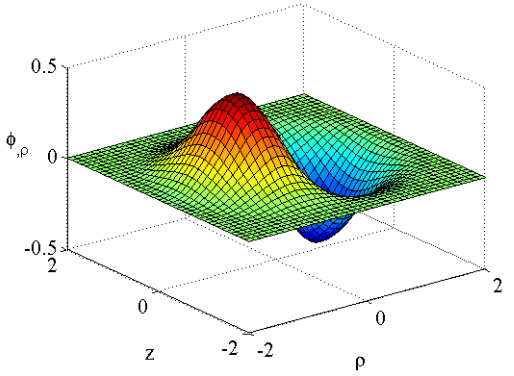

Fig. 3. First derivative of shape function, $\phi_{,\rho}$.

IV. THE MLPG ANALYSIS

The MLS function approximation is now applied to describe u in equation (5). The proposed analysis is similar to MLPG4/LBIE (local boundary integral equation) [2], but it differs in what concerns the imposition of boundary conditions, which follows the treatment of interface conditions discussed in [9]. For the MLPG method, it is necessary to spread nodes inside Ω (interior nodes) and over the global boundary $\partial\Omega$ (boundary nodes), as shown in Fig. 1. Interior nodes use the test function ψ_{I}, which acts in a local region near node I (the node's test domain $\Omega_{\mathrm{S_I}}$) where the integrations are carried out. In LBIE, $\Omega_{\mathrm{S_I}}$ is generally a circle centered at the interior node I and the corresponding test function ψ_{I} must satisfy the following requirements:

$$\nabla^2\psi_{\mathrm{I}} = -\delta(\mathrm{x}-\mathrm{x_I}) \text{ , a delta function at } \mathrm{x_I}, \quad (17)$$

$$\psi_I = 0, \text{ at the test domain boundary } \Omega_{\mathrm{S}}. \quad (18)$$

Conditions (17) and (18) are satisfied by the following test function:

$$\psi_{\mathrm{I}}(\mathrm{x}) = \frac{1}{2\pi}\ln\left(\frac{s_{\mathrm{I}}}{|\mathrm{x}-\mathrm{x_I}|}\right), \quad (19)$$

where s_{I} is the radius of the circular domain $\Omega_{\mathrm{S_I}}$, chosen such that $\Omega_{\mathrm{S_I}}$ does not intersect the global boundary $\partial\Omega$ [9]. The local weak form can be obtained by replacing ψ by ψ_{I} and u by u^h in (5), where the boundary integral vanishes due to (18), resulting in:

$$\iint_{\Omega_s} \frac{\nabla\psi_{\mathrm{I}}\cdot\nabla u^h}{f\rho}\,dA - k_0^2\iint_{\Omega_s}\frac{g\psi_{\mathrm{I}}u^h}{\rho}\,dA = 0. \quad (20)$$

This local formulation is versatile. For example, it can be used to analyze a layered medium of permissivities or permeabilities. In these cases, it is necessary to deal with the discontinuity between different media, which can be accomplished by using the techniques described in [11].

All boundary nodes are used to impose the boundary conditions and a simple technique (known as the meshless collocation scheme) that requires no integration is adopted [9]. Boundary conditions are expressed in a general form as:

$$b(\mathrm{x_I})u^h(\mathrm{x_I}) + c(\mathrm{x_I})\frac{\partial u^h(\mathrm{x_I})}{\partial n} = h(\mathrm{x_I}), \quad (21)$$

where $b = 1$ and $c = 0$ if $\mathrm{x_I}$ is at a Dirichlet boundary or $b = 0$ and $c = 1$ if it is at a Neumann boundary. h is a known imposed value. In a cavity with a perfect electric conductor wall, for TE modes, the function u satisfies a Dirichlet boundary condition over the wall (i.e. $E_\phi = 0$), while for TM modes a Neumann condition is imposed ($\partial H_\phi/\partial n = 0$). Over the axis of

symmetry (z-axis), the Dirichlet condition $u = 0$ is imposed for both modes, as $\rho = 0$.

The numerical solution of the problem is obtained by transforming (20) and (21) into a set of linear equations, resulting in:

$$(C - k_o^2 D)u_I = 0, \tag{22}$$

where, for interior nodes,

$$C_{\mathrm{IJ}} = \iint_{\Omega_S} \frac{\nabla\psi_{\mathrm{I}} \cdot \nabla\phi_{\mathrm{J}}}{f\rho}\, dA, \tag{23}$$

$$D_{\mathrm{IJ}} = \iint_{\Omega_S} \frac{g\psi_{\mathrm{I}}\phi_{\mathrm{J}}}{\rho}\, dA, \tag{24}$$

and, for boundary nodes, $C_{\mathrm{IJ}} = \phi_{\mathrm{J}}(\mathrm{x_I})$ (Dirichlet) or $C_{\mathrm{IJ}} = \partial\phi_{\mathrm{J}}(\mathrm{x_I})/\partial n$ (Neumann), and $D_{\mathrm{IJ}} = 0$. C and D are sparse matrices, which reduce the memory requirements and computation time by eliminating operations on zero elements. The wavenumbers k_0 are obtained from the eigenvalues of (22).

V. NUMERICAL RESULTS

Axially symmetric resonant cavities can be analyzed by the proposed technique. We present results for two cavities: a cylindrical and a spherical cavity. Only modes without ϕ-variation are analyzed (n = 0).

In the first example, we analyze a cylindrical cavity with radius equal to 1m, height equal to 2m, and vacuum in its interior ($\varepsilon_r = \mu_r = 1$). Table 1 shows the first resonant wavenumbers evaluated analytically [12] and numerically, using 3321 uniformly spaced nodes over the domain and its boundary (node spacing of 2.5cm). Table 1 also shows the percentual relative errors. The maximum error is approximately 0.49% for TM and 0.05% for TE modes. We do not have an explanation for the larger TM error. The main difference between the TE and TM problems is the boundary conditions: the TE problem only uses Dirichlet boundary conditions while the TM one has a Neumann boundary at the cavity wall. However, this difference does not completely explain the larger TM error.

In order to evaluate the convergence of the proposed method, it is necessary to determine the best values for the parameters α_{I}, which were defined in Section III to determine the node's influence domain. Our study demonstrated that the numerical accuracy depends on this parameter, with small α_{I} values leading to large errors because of the insufficient number of nodes to perform a precise MLS approximation. However, larger α_{I} values result in larger number of nodes inside the support domains. This results in an increase in time to evaluate the shape functions and in less sparse matrices, which also require more computing time to determine the eigenvalues and eigenvectors.

Table 1: Resonant wavenumbers k (rad/m) and relative errors (%) for the cylindrical cavity

$\mathbf{MODE_{npq}}$	Analytical Solution	Numerical Solution	Error (%)
TE_{011}	4.1411799	4.1423492	0.0282
$\mathbf{TE_{012}}$	4.9549545	4.9570499	0.0422
TE_{013}	6.0735970	6.0769282	0.0548
TM_{010}	2.4048255	2.4167237	0.4947
TM_{011}	2.8723835	2.8865461	0.4930
TM_{012}	3.9563607	3.9757341	0.4896

Figure 4 presents the relative error as a function of α_I. This figure (obtained with $N_{ini} = 6$ and 1981 uniformly spaced nodes over the domain and its boundary, with a node spacing of 33 cm) shows that optimum values of α_I are between 1.3 and 2.0. The simulations suggest the optimum values $\alpha_I = 1.3$ and 1.6 for TE and TM modes, respectively.

Figure 5 presents the convergence results for the six modes present in Table 1. The node spacing is changed in the interval [0.333 m, 0.025 m] and the convergence rates are approximately 1.84 and 1.2 for TE and TM modes, respectively.

Figures 6 through 8 present the electrical and magnetic field distributions inside the cavity, which were obtained extracting the field components from the eigenvectors using 1891 uniformly spaced nodes over the domain and its boundary (node spacing of 33 cm). Figure 6 shows $\mathrm{TE}_{011}(E_\phi)$ and $\mathrm{TM}_{010}(H_\phi)$ modes, Fig. 7 shows $\mathrm{TE}_{012}(E_\phi)$ and $\mathrm{TM}_{011}(H_\phi)$ modes, and Fig. 8 shows $\mathrm{TE}_{013}(E_\phi)$ and $\mathrm{TM}_{012}(H_\phi)$ modes. These numerical field distributions are in agreement with analytical results [12].

The second test problem is a spherical cavity with radius equal to 1 m and vacuum in its interior ($\varepsilon_r = \mu_r = 1$). Table 2 shows analytical [12] and numerical resonant wavenumbers ($n = 0$, with

2705 nodes uniformly spaced over the domain and its boundary, with node spacing of 2.5cm). The maximum error is approximately 0.69% for TM and 0.066% for TE modes.

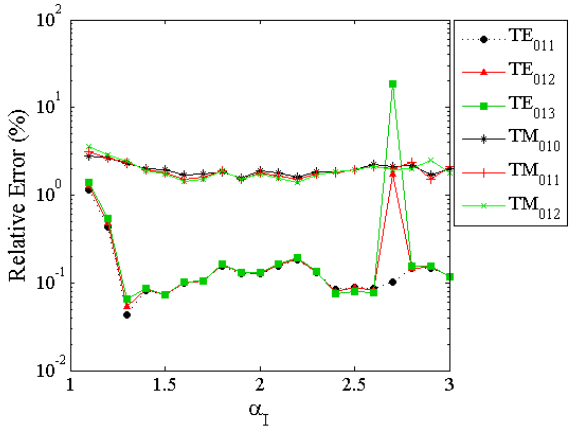

Fig. 4. Influence of the α_I values on the accuracy of the results for the cylindrical cavity.

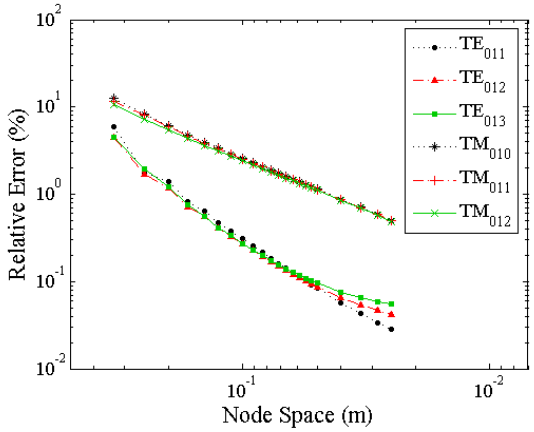

Fig. 5. Convergence of TE and TM modes for the cylindrical cavity.

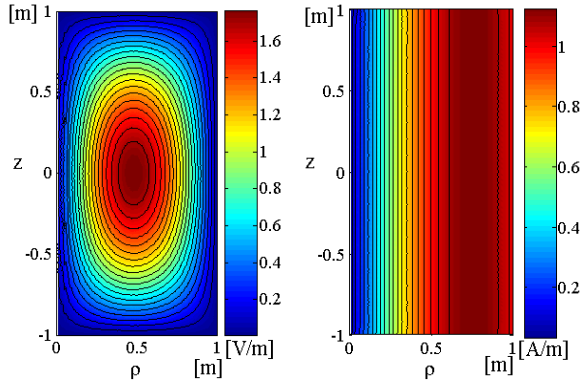

Fig. 6. Numerical field distribution in the cylindrical cavity: (a) $\mathrm{TE}_{011}(E_\phi)$ and $\mathrm{TM}_{010}(H_\phi)$.

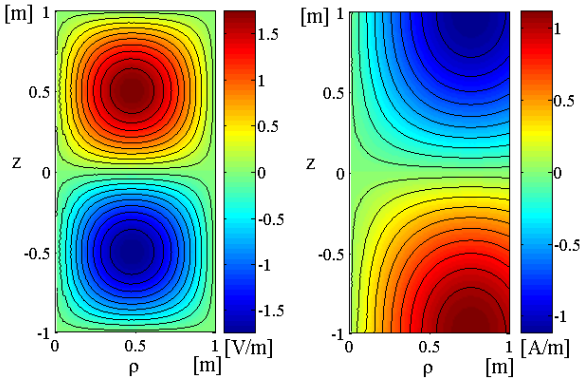

Fig. 7. Numerical field distribution in the cylindrical cavity: (a) $\mathrm{TE}_{012}(E_\phi)$ and $\mathrm{TM}_{011}(H_\phi)$.

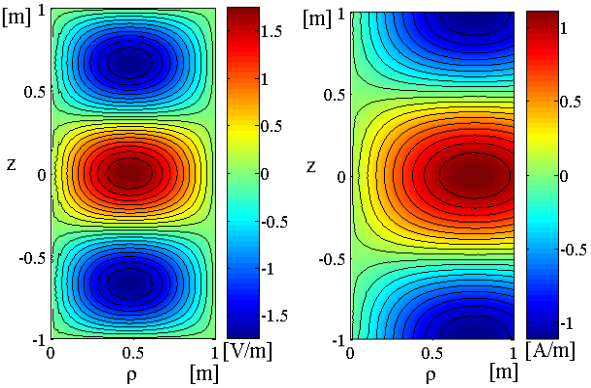

Fig. 8. Numerical field distribution in the cylindrical cavity: (a) $\mathrm{TE}_{013}(E_\phi)$ and $\mathrm{TM}_{012}(H_\phi)$.

Table 2: Resonant wavenumbers $k\ (rad/m)$ and relative errors (%) for the spherical cavity

$\mathbf{MODE_{npq}}$	**Analytical Solution**	**Numerical Solution**	**Error (%)**
TE_{011}	4.4934095	4.4949440	0.0341
$\mathbf{TE_{012}}$	5.7634592	5.7664633	0.0521
TE_{013}	6.9879300	6.9925602	0.0662
TM_{010}	2.7437072	2.7579069	0.5175
TM_{011}	3.8702386	3.8929146	0.5859
TM_{012}	4.9734204	5.0077221	0.6897

Figure 9 presents the convergence results for the modes present in Table 1 (built with the same N_{ini} and α_I values chosen for the cylindrical cavity). The convergence rates are approximately 2.0 and 1.4 for TE modes and TM modes, respectively.

Figures 10 through 11 present the numerical field distribution inside the spherical cavity, obtained using 1553 nodes uniformly spaced over the domain and its boundary (node spacing of

33cm). Figure 10 shows $\mathrm{TE}_{011}(E_\phi)$ and $\mathrm{TM}_{010}(H_\phi)$ modes, Fig. 11 shows $\mathrm{TE}_{012}(E_\phi)$ and $\mathrm{TM}_{011}(H_\phi)$ modes, and Fig. 12 shows $\mathrm{TE}_{013}(E_\phi)$ and $\mathrm{TM}_{012}(H_\phi)$ modes. Again, the field distributions are in perfect agreement with analytical results [12].

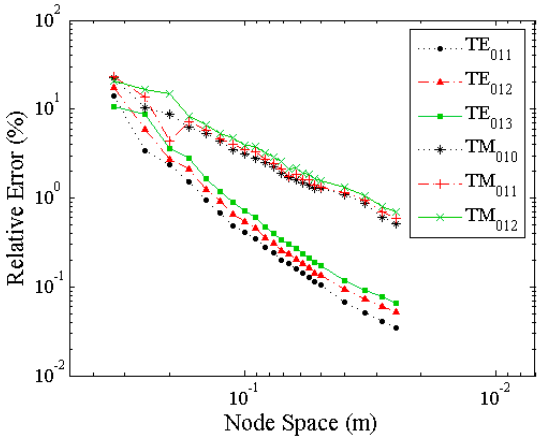

Fig. 9. Convergence of TE and TM modes for the spherical cavity.

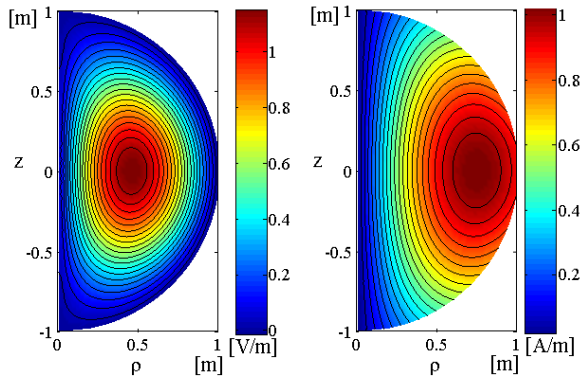

Fig. 10. Numerical field distribution in the spherical cavity: (a) $\mathrm{TE}_{011}(E_\phi)$ and $\mathrm{TM}_{010}(H_\phi)$.

CONCLUSIONS

This work discussed the numerical analysis of axisymmetric resonant cavities by a Meshless Local Petrov-Galerkin (MLPG) method. The axisymmetric weak formulation is simple and versatile. The proposed MLPG analysis uses a collocation method to impose the boundary conditions, which simplifies the algorithm. The employed method is a local weak-form method and does not require a background mesh.

Two axially symmetric resonant cavities had their eigenvalues and field distributions numerically evaluated. The proposed method had its convergence rate determined, which for a cylindrical cavity are 1.84 and 1.2 for TE and TM modes, respectively. For a spherical cavity, the convergence rates are 2 and 1.4 for TE and TM modes, respectively. The method can be easily adaptable to different axially symmetric geometries.

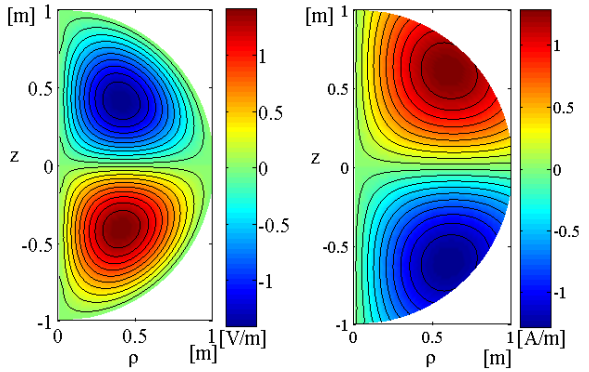

Fig. 11. Numerical field distribution in the spherical cavity: (a) $\mathrm{TE}_{012}(E_\phi)$ and $\mathrm{TM}_{011}(H_\phi)$.

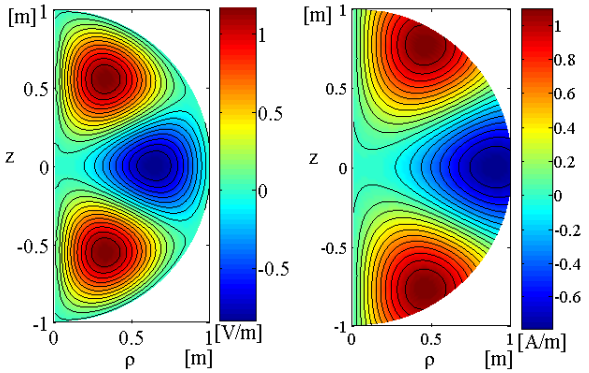

Fig. 12. Numerical field distribution in the spherical cavity: (a) $\mathrm{TE}_{013}(E_\phi)$ and $\mathrm{TM}_{012}(H_\phi)$.

ACKNOWLEDGMENT

This work was partially supported by CAPES, CNPq, and FAPEMIG.

REFERENCES

[1] A. Taflove and S. C. Hagness, *Computational Electrodynamics: The Finite-Difference Time-Domain Method, 3rd ed.* Norwood, MA: Artech House, 2005.

[2] G. Liu, *Mesh Free Methods: Moving Beyond the Finite Element Method*, CRC Press, 2nd Edition 2009.

[3] G. Ala, E. Francomano, A. Tortorici, E. Toscano, and F. Viola, "A Smoothed Particle Interpolation

Scheme for Transient Electromagnetic Simulation," *IEEE Trans. Magnetics*, vol. 42, no. 4, pp. 647-650, 2006.

[4] P. Jiang, S. Li, and C. Chan, "Analysis of Elliptical Waveguides by a Meshless Collocation Method with Wendland Radial Basis Functions," *Microwave and Optical Technology Letters*, vol. 32, no. 2, 2002.

[5] T. Kaufmann, C. Fumeaus, C. Engstrom, and R. Vahldieck, "Meshless Eigenvalue Analysis for Resonant Structures Based on the Radial Point Interpolation Method," *APMC 2009 Asia Pacific,* pp. 818-821, 2009.

[6] R. K. Gordon and W. E. Hutchcraft, "The Use of Multiquadric Radial Basis Functions in Open Region Problems," *Applied Computational Electromagnetic Society (ACES) Journal*, vol. 21, no. 2, pp. 127–134, July 2006.

[7] A. Manzin and O. Bottauscio, "Element-Free Galerkin Method for the Analysis of Electromagnetic-Wave Scattering," *IEEE Trans. Magnetics,* vol. 44, no. 6, pp. 1366-1369, 2008.

[8] B. Correa, E. Silva, A. Fonseca, D. Oliveira, and R. Mesquita, "Meshless Local Petrov-Galerkin in Solving Microwave Guide Problems," *IEEE Trans. Magnetics*, vol. 47, p. 1526-1529, 2011.

[9] W. Nicomendes, R. Mesquita, and F. Moreira, "A Meshless Local Petrov-Galerkin Method for Three-Dimensional Scalar Problems," *IEEE Trans. Magnetics*, vol. 47, pp. 1214-1217, 2011.

[10] A. Peterson, S. Ray, and R. Mittra, *Computational Methods for Electromagnetics*, IEEE Press, 1998, Sect. 8.8.

[11] Q. Li, S. Shen, Z. Han, and S. Atluri, "Application of Meshless Local Petrov-Galerkin (MLPG) to Problems with Singularities, and Material Discontinuities, in 3-D Elasticity," CMES, vol. 4, no. 5, pp. 571-585, 2003.

[12] R. F. Harrington, *Time-Harmonic Electromagnetic Fields*; McGraw-Hill, New York, 1961.

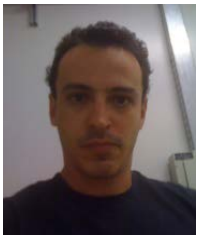

Ramon Dornelas Soares received his Bachelor's and Master's degrees from the National Institute of Telecommunication (INATEL), Santa Rita do Sapucai, Brazil, in 2002 and 2005. He is currently working towards his Doctor's degree in Electrical Engineering at the Federal University of Minas Gerais, Brazil. His main research interests are in the area of electromagnetic field computation.

Renato Cardoso Mesquita is a professor at the Electrical Engineering Department of the Federal University of Minas Gerais, Brazil. He received his B.E. and M.Sc. degrees from the Federal University of Minas Gerais, in 1982 and 1986, and his Ph.D from the Federal University of Santa Catarina, Brazil, in 1990. His main research interests are in the area of electromagnetic field computation.

Fernando José da Silva Moreira was born in Rio de Janeiro, Brazil, in 1967. He received the B.S. and M.S. degrees in Electrical Engineering from the Pontifical Catholic University of Rio de Janeiro, Brazil, in 1989 and 1992, and the Ph.D. degree in Electrical Engineering from the University of Southern California in 1997. Since 1998, he has been with the Department of Electronics Engineering of the Federal University of Minas Gerais, Brasil, where he is currently an Associate Professor. His research interests are in the areas of electromagnetics, antennas, and propagation.